Chapter 4
Buck-boost converter fault diagnosis for an EDF-100 distillation pilot plant

Mario Heras Cervantes[1], Adriana del Carmen Téllez Anguiano[1], and Juan Anzurez Marin[2]

Abstract Distillation is the process of separating chemical mixtures most commonly used in industry, with applications ranging from cosmetic and pharmaceutical to petrochemical industries. The equipment used to perform the distillation process is the distillation column. Initial investment and maintenance costs for distillation columns are very high; therefore, it is necessary to have an appropriate fault detection system that allows improving the safety and security of the diverse parts of the column including the heating subsystem, which generates the caloric power necessary to evaporate the mixture. This work presents a fault detection and diagnosis algorithm for the heating subsystem that is implemented by using a buck-boost converter and by using the Takagi-Sugeno fuzzy model. Practical considerations related to the implementation, analysis and a comparison of the results of the convert obtained from simulated and experimental data in a distillation column using a binary mixture (of ethanol and water) are presented.

4.1 Introduction

The dependence of modern society on technological systems and processes has increased in recent years; therefore, the proper functioning of these systems has become a necessity. On the other hand, industrial systems and processes are increasingly sophisticated because of their components and the functions that they implement. This increases their vulnerability to faults, however (Verde et al., 2013; Kordestani et al., 2019; Demidova et al., 2021).

Generally, a fault is an undesired variation in the normal behavior of the system, causing damage to the equipment and risks for the user as well as products with undesired characteristics (Verde et al., 2013).

The vast majority of control systems do not consider factors such as the malfunction of sensors, actuators or other components that can cause inadequate behavior of the system and instability or risks for the users. Therefore, industrial processes need to implement feedback and automation devices that allow better performance and greater safety (Zhong et al., 2017; Bahreini et al., 2021; Iqbal et al., 2019).

In recent years, the design of fault detection and isolation (FDI) systems has been proposed in order to detect faults and maintain stability and desired performance. Reliable, timely and efficient fault detection

[1]Tecnológico Nacional de México/Instituto Tecnológico de Morelia, Av. Tecnológico 1500, Col. Lomas de Santiaguito, Morelia, Michoacán, Mexico, e-mail: mario.hc@morelia.tecnm.mx and adriana.ta@morelia.tecnm.mx

[2]Universidad Michoacana de San Nicolás de Hidalgo, Santiago Tapia 403, Centro, Morelia, Michoacán, Mexico e-mail: juan.anzurez@umich.mx

can prevent risks for both the process and the user, which is why fault detection techniques in industrial systems have become indispensable.

At an industrial level, various processes require an FDI system to operate properly. In the particular case of the chemical industry, distillation is a process that can benefit from these systems since it requires a large amount of energy to heat the mixture. The malfunction of a component can affect the safety of the operators or the quality of the product, hence the need to implement constant monitoring techniques to avoid faults in the process (Ming and Zhao, 2017; Khan et al., 2020; Ankur et al., 2020).

In a distillation column, the process of separating one or more components of a mixture is performed from their difference in volatility, which requires an actuator to generate the caloric power necessary to evaporate the mixture. The most common actuators for this purpose are based on power electronics converters that regulate the voltage or current in the electric heating resistance responsible for generating this caloric power.

In this chapter, an FDI system applied to a buck-boost converter was developed. This converter regulates the heating power, Q_b, through the electrical power, W, in a heating resistance through the duty cycle, d, of a Pulse Width Modulation power signal in an EDF-1000 distillation pilot plant. For the sake of contextualization, the distillation column model is described in Section 4.2. The developed FDI system is composed of two fuzzy observers with sliding modes that estimate the output voltage of the converter (v_C) and the current in the inductor (i_L). With the estimation errors of each observer, the residuals r_1 and r_2 are generated, respectively, to determine the symptoms that indicate the presence or absence of a fault. The system validation is performed in simulation and uses experimental data in real-time on an EDF-1000 distillation pilot plant.

4.2 Model of a distillation column and its heating actuator

In industry, distillation is the process most commonly used to separate chemical mixtures, with the petrochemical (production of petroleum derivatives) and food (production of alcoholic beverages) industries being the most important, because of the current lifestyle of people (Ibrahim et al., 2018).

The objective of distillation is to separate two or more elements from a mixture, where the most volatile element is obtained as a distilled product. The equipment to carry out the distillation process is the distillation column or the distillation pilot plant, as shown in Fig. 4.1, which is composed of a condenser, a boiler and the body of the column consisting of multiple perforated plates.

The boiler is the element that provides the necessary heat for evaporating the liquid mixture contained in it. The vapor flow, as it moves up the plates of the column body, is enriched by the light element, i.e., the element with the lowest boiling point in the mixture. The vapor that reaches the condenser is condensed and, according to the state of the reflux valve, is extracted as a distilled product or re-enters the column. The liquid that re-enters through the reflux action descends by gravity into the body of the column, enriched with the heavy element, i.e., the element with the highest boiling point. Each plate of the distillation column corresponds to a degree of purity of the light element known as molar fraction (Téllez, 2010). Because of the cost of the required sensors or meters, the mole fraction is measured off-line.

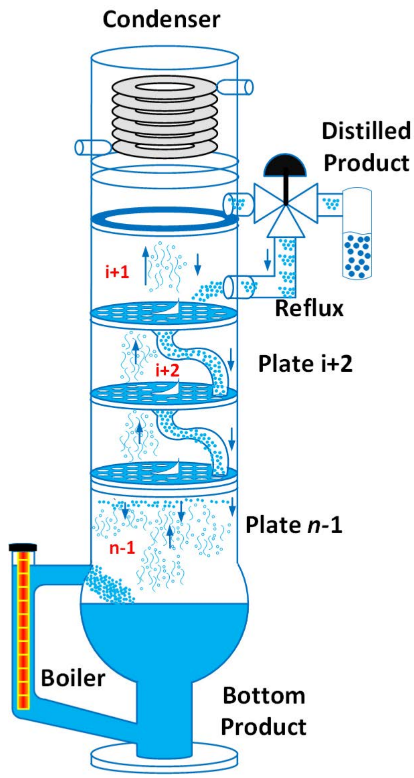

Fig. 4.1: Distillation column schematic

Fractional distillation is used to separate homogeneous liquid mixtures where the components have a difference between their boiling points of less than 25 ^{o}C. Generally, there are two operation modes of fractional distillation, named continuous and batch. In the continuous mode, the feeding of the liquid mixture and the extraction of the distilled product is performed continuously.

In batch distillation, the mixture is deposited in the boiler. At the end of the process, the distillate and bottom product are extracted; the batch operation mode is mainly used to separate small amounts of mixture, obtain different qualities of the distilled product for the same mixture or separate multicomponent mixtures.

A batch distillation column is not operated with constant parameters, but rather the control actions are continuously adjusted according to the state of the distillation. Therefore, the continuous and correct monitoring and control of all the variables of the process are essential for improving the quality and quantity of the distilled product, as well as the safety of the process and the users. To achieve this objective, it is necessary to have models and apply the design of observers and FDI systems.

The actuators in a distillation column have a very important role because they can modify physical variables of the process such as temperature and pressure (Paraschiv and Olteanu, 2015), by modifying the purity of the product from reflux (Alhaboubi et al., 2022) or the distillation rate.

Figure 4.2 shows the instrumentation diagram of a distillation pilot plant that includes the temperature sensors, as well as the actuator scheme with the heating power control that regulates the amount of heat in the boiler.

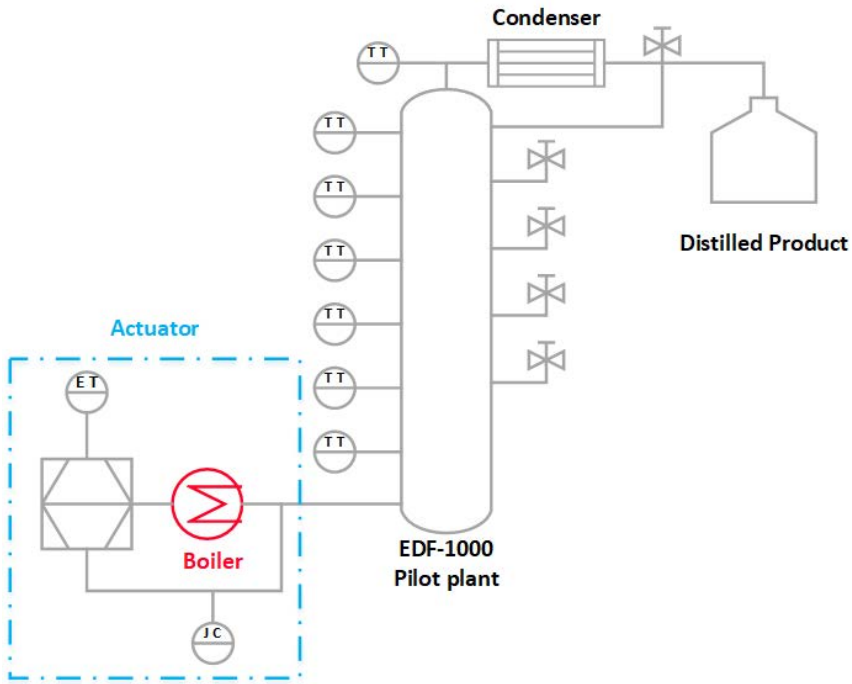

Fig. 4.2: Instrumentation diagram of the EDF-1000 distillation pilot plant. TT, TV and LP are the temperature transmitter, the voltage transmitter and power control, respectively

4.2.1 Nonlinear model of the distillation column

The distillation column model consists of a set of differential equations that represent the dynamics of each plate of the column in steady state, i.e., when the first drop is distilled. Generally, the model of a distillation column is based on the balance of the light component in the plates and is given by

$$\frac{dx_i}{dt} = \frac{V_d(g_{i+1} - g_i) + L_d(x_{i-1} - x_i)}{M_i}, \tag{4.1}$$

for $i = 2, 3, \ldots, n-1$, where V_d is the vapor molar flow, L_d the liquid molar flow, M_i the retained mass in plate i, $x_{i\pm m}$ the liquid composition in plate $i \pm m$, $g_{i\pm m}$ the vapor composition in plate $i \pm m$ with $m = 1$ and each component x_i, $g_i \in \mathbb{R} : 0 < x_i \leq 1, 0 < g_i \leq 1$.

For $i = 1$, the condenser schematic named plate 1 is shown in Fig. 4.3, and its dynamics is expressed by

$$\frac{dx_1}{dt} = \frac{V_d g_2 - L_d x_1 - D x_1}{M_1}, \tag{4.2}$$

where M_1 is the retained mass in the condenser, x_1 is the liquid composition in the condenser, g_1 is the vapor composition in the condenser, and D is the distilled product.

Thus, the body of the column is formed by $n-2$ plates. Figure 4.4 shows the schematic of a plate in the body of the column, as well as the variables that interact in the dynamics of each plate, which are expressed by (4.1).

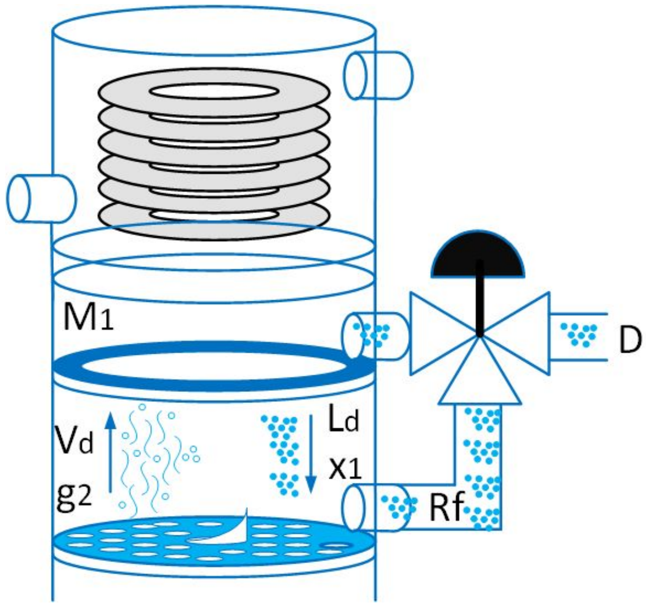

Fig. 4.3: Condenser schematic

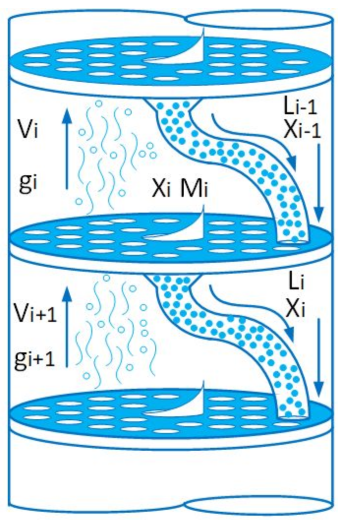

Fig. 4.4: Plate schematic

Figure 4.5 shows the schematic of the boiler in the distillation column for the plate n and its dynamics is expressed by

$$\frac{dx_n}{dt} = \frac{V_d x_n - V_d g_n + L_d x_{n-1} - L_d x_n}{M_n}, \tag{4.3}$$

where M_n is the retained mass in the boiler, x_n the liquid composition in the boiler, g_n the vapor liquid composition in the boiler, x_{n-1} the liquid composition in plate $n-1$ and n the total number of plates.

Additionally, according to Skogestad (1997), a batch type distillation column has an interaction of three molar flows:

- vapor, V_d

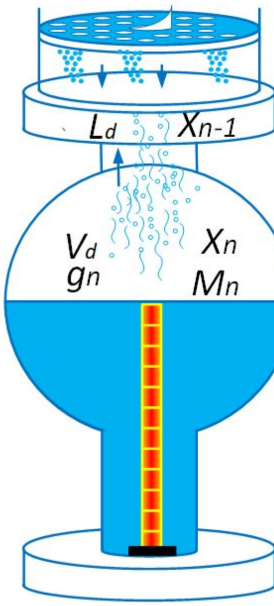

Fig. 4.5: Boiler schematic

$$V_d = \frac{Q_b}{H_i^{vap} x_n + H_j^{vap}(1 - x_n)}, \tag{4.4}$$

where Q_b is the heating power, H_i^{vap} the vapor enthalpy of the light element of the mixture and H_j^{vap} the vapor enthalpy of the heavy element of the mixture.

- liquid, L_d

$$L_d = (1 - Rf)V_d, \tag{4.5}$$

where Rf the percentage of the reflux action.

- distilled product, D

$$D = V_d - L_d. \tag{4.6}$$

In addition, the relative volatility is considered dynamic, i.e., changes over time, in the model presented in this chapter. Relative volatility is defined as the difference between the vapor pressure of the most volatile components and the vapor pressure of the less volatile components of a liquid mixture, expressed in

$$g_i P_T = P_i^{sat} x_i \gamma_i, \tag{4.7}$$

where P_i^{sat} is the saturation pressure of the mixture components, γ_i is the activity coefficient and P_T is the total pressure of the process expressed in the liquid-vapor equilibrium for nonideal mixtures. The activity coefficient γ_i is dependent on the liquid concentration of the elements in the mixtures.

4.3 Case study: EDF-1000 distillation pilot plant

The case study is the EDF-1000 distillation pilot plant shown in Fig. 4.6, consisting of 11 perforated plates, 7 of which have Pt100 RTD temperature sensors located in the condenser (plate 1), plates 2, 4, 6, 8, 10 and the boiler (plate 11).

Fig. 4.6: EDF-1000 distillation pilot plant

The most important physical characteristics of the EDF-1000 distillation pilot plant are as follows:

- Two-liter boiler tank
- 350-Watts heating resistor
- Bottom product output valve
- Double spiral-condenser
- On-off reflux valve

4.3.1 State-space model of the EDF-1000 distillation pilot plant

In order to obtain the linear state-space model of the EDF-1000 distillation pilot plant with 11 plates for a binary mixture, and considering that $g_i = (1 - x_i)$, $G(x_i)$ is expressed for any operation point as

$$G(x_i) = x_i \frac{P_i^{sat} e^{A_{21}\left(\frac{A_{21}(1-x_i)}{A_{12}x_i + A_{21}(1-x_i)}\right)^2}}{P_T}. \tag{4.8}$$

Thus, the model can be represented by

$$\dot{x} = \begin{pmatrix} \frac{-(V_d+D)}{M_1} & \frac{V_d \cdot G(x_1)}{M_1} & 0 & \dots & 0 \\ \frac{L_d}{M_2} & \frac{-V_d \cdot G(x_2)-L_d}{M_2} & 0 & \dots & 0 \\ \vdots & \vdots & \ddots & \vdots & \vdots \\ 0 & 0 & \dots & \frac{-V_d \cdot G(x_{10})-L_d}{M_{10}} & \frac{V_d \cdot G(x_{11})}{M_{10}} \\ 0 & 0 & \dots & \frac{L_d}{M_{11}} & -\frac{L_d}{M_{11}} \end{pmatrix} x + \begin{pmatrix} \frac{V_d x_1}{M_1} & 0 \\ 0 & 0 \\ \vdots & \vdots \\ 0 & 0 \\ 0 & \frac{x_n(1-G(x_n))}{(H^{vap}_{etha} x_n + H^{vap}_{H2O}(1-x_n)M_n)} \end{pmatrix} \begin{pmatrix} R_f \\ Q_b \end{pmatrix}. \tag{4.9}$$

where the light component compositions, $x^T = [x_1, x_2, \cdots, x_{10}, x_{11}]$ are the state deviations with respect of the operation point and the heating power, Q_b, the reflux, R_f, the control inputs and A_{21} and A_{12} are the activity coefficients of the mixture components.

The system output is given by

$$y = Cx = Ix, \tag{4.10}$$

with I the identity matrix. These equations are described in detail in (Orozco et al., 2016).

The following considerations for the distillation column are assumed.

- Constant pressure throughout the column
- Inflows and outflows in the liquid state
- No vapor retention
- Vapor and liquid balance
- Vapor and liquid perfectly mixed
- Adiabatic distillation column
- Batch feeding

The simulation results of these nonlinear models are described in Orozco et al. (2016).

4.3.2 EDF-1000 heating actuator scheme and model

The boiler is the element that provides the amount of heat necessary to evaporate the mixture to be distilled. Boiler actuators generally control heating power from electricity. The amount of the generated heat output allows controlling the distillation rate in the process, according to equations (4.4) to (4.6), as shown in Fig. 4.7.

It is very important to regulate the temperature at a suitable value because in certain mixtures different temperatures represent different products, as in the case of petroleum distillation. An inadequate generation of the heat exchange between the boiler and the mixture in the distillation process can cause temperature variations, no-uniform heating in the mixture and thermal shocks in the plates, among other damage. Therefore, it is important to design FDI systems to avoid risks for the user and damage to the equipment (Paraschiv and Olteanu, 2015).

The boiler in the case study is formed by two tanks where the mixture is deposited and heated by a heating element (resistor). Figure 4.8 shows the schematic of the two-tank boiler.

The heating power is determined by Joule's Law expressed as follows: The amount of heat generated by an electric current passing through a conductor is directly proportional to the resistance of the

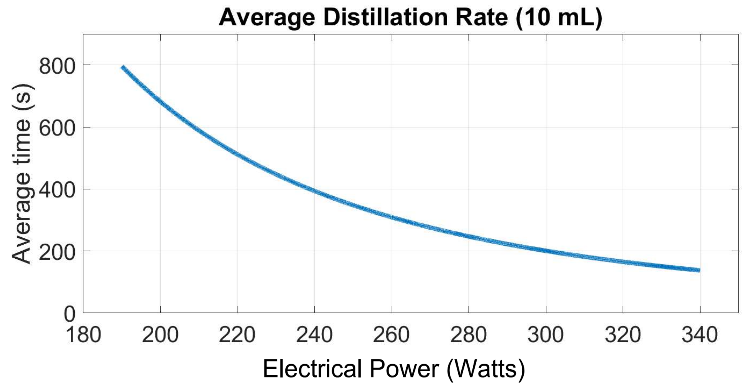

Fig. 4.7: Distillation rate versus electrical power

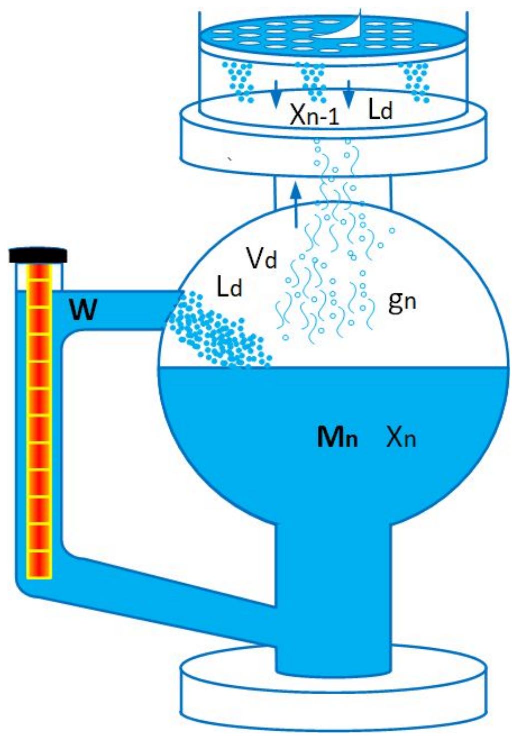

Fig. 4.8: Two-tank boiler schematic

conductor, the square of the intensity of the current and the duration of the current passing through the conductor (Li et al., 2022). Joule's law is described by

$$J = {i_e}^2 R t, \tag{4.11}$$

where J is the heat amount (Joules), i_e the electric current (Amperes), R the resistance (Ohms) and t the time (seconds).

The law of conservation of energy states that energy cannot be created or destroyed; it can only be changed from one form to another. Joule's law expressed in electrical power W is defined by

$$J = Wt. \tag{4.12}$$

The heating resistance converts the electric energy into heat by the circulation of current. Therefore, the boiler heating power can be manipulated and modeled from the electrical power in the resistance, i.e., in the heating actuator of a distillation column, Q_b is expressed as

$$Q_b = Wt. \tag{4.13}$$

The boiler actuator scheme, shown in Fig. 4.9, adjusts the output power W_o in the boiler heating resistance by regulating the output voltage V_o with a DC-DC converter. DC-DC converters can regulate the output voltage to the desired value by switching electronic devices, usually diodes and transistors. These power electronics converters have applications in renewable energy systems, smart grids, as well as domestic and laboratory equipment power systems (Affam et al., 2021; Rojas et al., 2018).

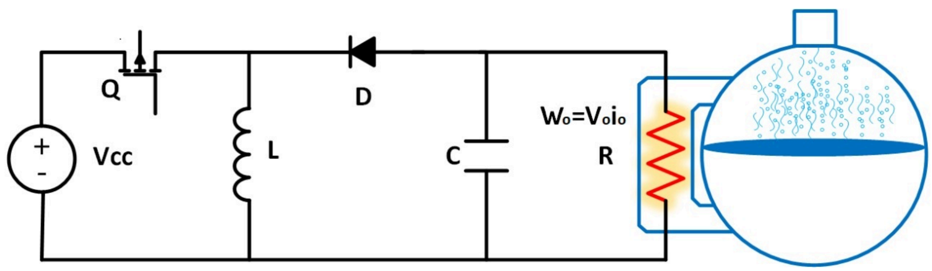

Fig. 4.9: Boiler actuator scheme using a buck-boost converter

The basic topologies of CD-CD converters are buck, boost and buck-boost (Rashid, 2017). In the buck converter, the output voltage is lower than the input voltage; in the boost converter the output voltage is greater than the input voltage.

The buck-boost converter is a combination of both converters depending on the duty cycle service d, where the output voltage V_o is given by (4.14). For d values less than 0.5, the configuration corresponds to a buck converter. On the contrary, d greater than 0.5 corresponds to a boost converter

$$V_o = -\frac{V_{cc}d}{1-d} \qquad \text{with } 0 < d < 1. \tag{4.14}$$

Input voltage, load variations, disturbances and deterioration of the power converters components (Tarakanath et al., 2014), are undesired factors that directly affect their performance, reliability and safety, hence the importance of designing and implementing FDI strategies that facilitate estimating or identifying fundamental parameters in its operation to improve safety and reliability in the system.

4.3.2.1 Buck-boost converter linear model

The linear model of the buck-boost converter is obtained from the ON - OFF states of the switching device (transistor), considering the set of equations from each topological state. The matrix representation of the model is given by

$$\begin{pmatrix} \dot{i}_L \\ \dot{v}_C \end{pmatrix} = A \begin{pmatrix} i_L \\ v_C \end{pmatrix} + Bu, \tag{4.15}$$

where the state variables are the inductor current i_L and the capacitor voltage v_C.

During the ON-state time ($t = ON$) the converter has the topological circuit shown in Fig. 4.10, and its model is written as

$$\begin{pmatrix} \dot{i}_L \\ \dot{v}_C \end{pmatrix} = \begin{pmatrix} 0 & 0 \\ 0 & -\frac{1}{RC} \end{pmatrix} \begin{pmatrix} i_L \\ v_C \end{pmatrix} + \begin{pmatrix} \frac{1}{L} \\ 0 \end{pmatrix} V_{cc}. \tag{4.16}$$

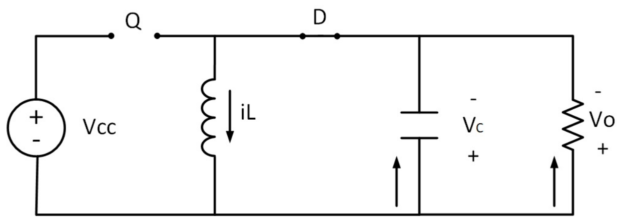

Fig. 4.10: Topological ON-state of the buck-boost converter

During the OFF-state time ($t = OFF$), the converter has the topological circuit shown in Fig. 4.11, and its model is described as

$$\begin{pmatrix} \dot{i}_L \\ \dot{v}_C \end{pmatrix} = \begin{pmatrix} 0 & \frac{1}{L} \\ -\frac{1}{C} & -\frac{1}{RC} \end{pmatrix} \begin{pmatrix} i_L \\ v_C \end{pmatrix} + \begin{pmatrix} 0 \\ 0 \end{pmatrix} V_{cc}. \tag{4.17}$$

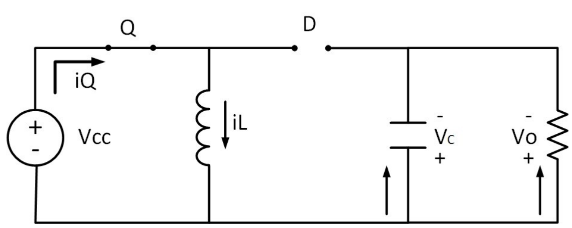

Fig. 4.11: Topological OFF-state of the buck-boost converter

The main characteristic of this model is the commutation between the two linear subsystems, represented by (4.16) and (4.17), which commute from the state of the Q switch. The general matrix representation of the system (4.15) is expressed in

$$\begin{pmatrix} \dot{i}_L \\ \dot{v}_C \end{pmatrix} = A_k \begin{pmatrix} i_L \\ v_C \end{pmatrix} + B_k u, \tag{4.18}$$

where $k = 1, 2$ characterize the subsystem for each state of the transistor. Thus,

$$A_1 = \begin{pmatrix} 0 & 0 \\ 0 & -\frac{1}{RC} \end{pmatrix}, \; A_2 = \begin{pmatrix} 0 & \frac{1}{L} \\ -\frac{1}{C} & -\frac{1}{RC} \end{pmatrix}, \; B_1 = \begin{pmatrix} \frac{V_s}{L} \\ 0 \end{pmatrix}, \; B_2 = \begin{pmatrix} 0 \\ 0 \end{pmatrix}, \; x = \begin{pmatrix} i_L \\ v_C \end{pmatrix}.$$

4.3.2.2 Buck-boost converter nonlinear model

The nonlinear model of the converter unifies both linear subsystems and includes the control variable u, which is determined by the duty cycle $u = d$ by considering values between 0 and 1, as shown in

$$\begin{pmatrix} \dot{i}_L \\ \dot{v}_C \end{pmatrix} = \left(A_1 \begin{pmatrix} i_L \\ v_C \end{pmatrix} + B_1\right) d + \left(A_2 \begin{pmatrix} i_L \\ v_C \end{pmatrix} + B_2\right)(1-d). \tag{4.19}$$

This equation can be also represented as

$$\begin{pmatrix} \dot{i}_L \\ \dot{v}_C \end{pmatrix} = A_2 \begin{pmatrix} i_L \\ v_C \end{pmatrix} + B_2 + (A_1 - A_2) \begin{pmatrix} i_L \\ v_C \end{pmatrix} d + (B_1 - B_2) d. \tag{4.20}$$

This model is considered an average model of the linear submodels. As can be observed from (4.16) to (4.20), the capacitor voltage v_C can be affected by variations in the load (heating resistor) and the input voltage, provoking faults in the actuator and, hence, in the distillation column dynamics.

4.3.2.3 Buck-boost converter Takagi-Sugeno linear model

A Takagi-Sugeno (TS) fuzzy model that interpolates between p linear submodels is based on the following model rule:

Model Rule i:
if $z_1(t)$ is M_{i1} and ... and $z_p(t)$ is M_{ip}
Then

$$\begin{aligned} \dot{x}(t) &= A_i x(t) + B_i u(t) \\ y &= C_i x(t), \end{aligned} \tag{4.21}$$

where $z_i(t) \in \mathbb{R}^p$ are the fuzzy variables, M_{ip} the fuzzy sets, $x(t) \in \mathbb{R}^n$ the state vector, $u(t) \in \mathbb{R}^r$ the input vector, $y(t) \in \mathbb{R}^m$ the measurable output vectors, $C \in \mathbb{R}^{m \times n}$ an output matrix, and the matrices $A_i \in \mathbb{R}^{n \times n}$ and $B_i \in \mathbb{R}^{n \times r}$, for all i, the state and input matrices with real finite values.

Based on the nonlinear model of the buck-boost converter, presented in (4.20), and using as fuzzy variables the states ($z_1 = v_C$, $z_2 = i_L$) that operate between maximum and minimum nominal values ($z_{1max} = v_{C_{max}}$, $z_{1min} = v_{C_{min}}$, $z_{2max} = i_{L_{max}}$, $z_{2max} = i_{L_{min}}$), a Takagi-Sugeno fuzzy model that interpolates between four linear submodels based on the following rules is proposed.

According to the converter characteristics, the linear submodels are obtained using a nonlinear sector condition, where

$$A_1 = \begin{pmatrix} 0 & 1/L \\ -1/C & -1/RC \end{pmatrix} = A_2 = A_3 = A_4$$

$$B_1 = \begin{pmatrix} \frac{V_{in}+z_{1_{min}}}{L} \\ \frac{z_{2_{min}}}{C} \end{pmatrix}, \quad B_2 = \begin{pmatrix} \frac{V_{in}+z_{1_{min}}}{L} \\ \frac{z_{2_{max}}}{C} \end{pmatrix}, \quad B_3 = \begin{pmatrix} \frac{V_{in}+z_{1_{max}}}{L} \\ \frac{z_{2_{min}}}{C} \end{pmatrix}, \quad B_4 = \begin{pmatrix} \frac{V_{in}+z_{1_{max}}}{L} \\ \frac{z_{2_{max}}}{C} \end{pmatrix}$$

$$C_1 = \begin{pmatrix} 1 & 0 \\ 0 & 1 \end{pmatrix} = C_2 = C_3 = C_4.$$

To describe the fuzzy sets for the capacitor voltage $v_C = z_1$ the membership functions $\mu(z_1)$ are used

$$\mu_{z_{1min}}(z_1) = \begin{cases} 1 & if \;\; z_1 \le z_{1min} \\ \frac{z_{1max}-z_1}{z_{1max}-z_{1min}} & if \;\; z_{1min} < z_1 < z_{1max} \\ 0 & if \;\; z_1 \ge z_{1max}; \end{cases}$$

$$\mu_{z_{1max}}(z_1) = \begin{cases} 0 & if \;\; z_1 \le z_{1min} \\ 1-\mu_{z_{1_{min}}} & if \;\; z_{1min} < z_1 < z_{1max} \\ 1 & if \;\; z_1 \ge z_{1max}; \end{cases}$$

and for the inductor current $i_L = z_2$ by

$$\mu_{z_{2min}}(z_2) = \begin{cases} 1 & if \;\; z_2 \le z_{2min} \\ \frac{z_{2max}-z_2}{z_{2max}-z_{2min}} & if \;\; z_{2min} < z_2 < z_{2max} \\ 1 & if \;\; z_2 \ge z_{2max} \end{cases}$$

$$\mu_{z_{2max}}(z_2) = \begin{cases} 0 & if \;\; z_2 \le z_{2min} \\ 1-\mu_{z_{2_{min}}} & if \;\; z_{2min} < z_1 < z_{2max} \\ 1 & if \;\; z_2 \ge z_{2max}. \end{cases}$$

The normalized weights h_i are given by

$$\begin{aligned} h_1(z_1,z_2) &= \mu_{z_{1min}}(z_1)\mu_{z_{2min}}(z_2), \quad h_2(z_1,z_2) = \mu_{z_{1min}}(z_1)\mu_{z_{2max}}(z_2), \\ h_3(z_1,z_2) &= \mu_{z_{1max}}(z_1)\mu_{z_{2min}}(z_2), \quad h_4(z_1,z_2) = \mu_{z_{1max}}(z_1)\mu_{z_{2max}}(z_2). \end{aligned}$$

Thus, the Takagi-Sugeno fuzzy model for the buck-boost converter, considering $r = 4$, A constant and $d = u(t)$ is given by

$$\begin{aligned} \dot{x}(t) &= Ax(t) + \left. \sum_{i=1}^{r} h_i(z_1,z_2)B_i \right) d \\ y(t) &= \sum_{i=1}^{r} h_i(z_1,z_2)C_i x(t). \end{aligned} \tag{4.22}$$

4.4 Observers design

A state observer is a dynamic system that estimates state variables or parameters from available measurements. Observers, also called virtual sensors, are widely used because they estimate the system variables that are not measurable by using mathematical algorithms and available measurements. An advantage of the observer is that it can detect and locate faults in the system. In addition, it is a systematic design procedure, which facilitates its implementation and execution in real time.

The precise mathematical model of the system to be estimated is a key point in the design since the observer recovers the behavior of the real system from its model using a closed loop scheme. (Lopez et al., 2015; Téllez-Anguiano et al., 2017; Heras-Cervantes et al., 2016). The general dynamic observer for estimating the states is

$$\dot{\hat{x}}(t) = \underbrace{A\hat{x} + Bu(t)}_{Predictor} + \underbrace{L(y(t) - \hat{y}(t))}_{Corrector}, \tag{4.23}$$

where $\hat{x}$ in $\mathbb{R}^n$ represents the state estimate for all time $\tau > t_0$ and the estimated output is given by $\hat{y}(t) = C\hat{x}(t)$.

The system presented in (4.23) is also denoted as the Luenberger identity observer and is coupled with the original process through the inputs and outputs, as shown in Fig. 4.12. The observer consists of two parts: a predictive stage, based on the model of the observed system, and a corrective stage, formed by the estimation error $e(t) = y(t) - \hat{y}(t)$, i.e., the difference between the measurable and estimated outputs.

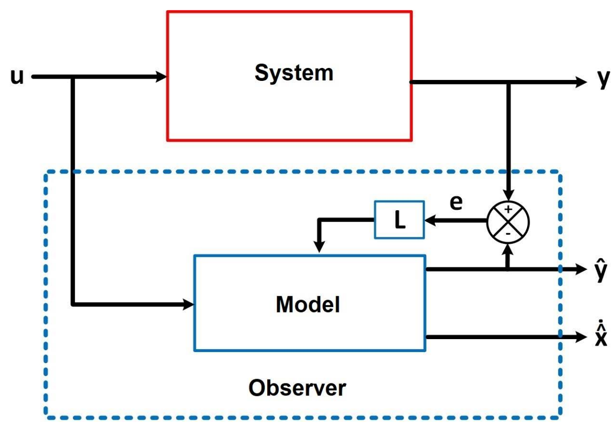

Fig. 4.12: General scheme of a state observer

4.4.1 Takagi-Sugeno fuzzy observer

Combining the Takagi-Sugeno fuzzy model of a nonlinear system with the Luenberger observer, the general structure of a fuzzy observer is obtained, according to Tanaka et al. (1998), as

$$\begin{aligned} \dot{\hat{x}}(t) &= \sum_{i=1}^{r} h_i(z(t))[A_i\widehat{x}(t) + B_i u(t) + K_i e] \\ \widehat{y}(t) &= \sum_{i=1}^{r} h_i(z(t))C_i\widehat{x}(t). \end{aligned} \tag{4.24}$$

In Nguyen et al. (2019), the authors demonstrate the stability of the fuzzy observer as long as there is a P matrix that satisfies the linear matrix inequalities (LMIs) given by

$$\begin{gathered} P > 0 \\ N_i > 0 \\ A_i^T P - C_i^T N_i^T + PA_i - N_i C_i < 0 \\ A_i^T P - C_j^T N_i^T + PA_i - N_i C_j + PA_j^T - C_i^T N_j^T + PA_j - N_j C_i < 0, \end{gathered} \tag{4.25}$$

where P and N_i are positive definite matrices $P > 0, N_i > 0$ and the condition should be hold for all $i < j$. Observer gains are defined by the LMI's system solution defined in

$$K_i = P_o^{-1} N_i. \tag{4.26}$$

4.4.2 Sliding-Mode fuzzy observer

The sliding-mode fuzzy observer is based on the Luenberger observer for linear systems and the fuzzy observer proposed by Tanaka et al. (1998). By using a fuzzy observer, sliding-mode local observers can be built for each linear subsystem. Each observer is associated with a fuzzy rule i defined by

$$\begin{gathered} \textbf{Fuzzy Rule i}: \\ \textbf{if } z_1(t) \text{ is } M_{i1} \text{ and ... and } z_p(t) \text{ is } M_{ip} \\ \textbf{Then} \\ \dot{\hat{x}}(t) = A_i \hat{x}(t) + B_i u(t) + K_i e + \varphi_i(t) \\ \hat{y} = C_i \hat{x}(t). \end{gathered} \tag{4.27}$$

The final observer is given by the weighted sum of each subsystem, as shown in

$$\begin{gathered} \dot{\hat{x}}(t) = \sum_{i=1}^{r} h_i(z(t))(A_i \hat{x}(t) + B_i u(t) + K_i(e) + \varphi_i(t)) \\ \hat{y}(t) = \sum_{i=1}^{r} h_i(z(t))(C\hat{x}(t)). \end{gathered} \tag{4.28}$$

The term $\varphi_i(t)$ is the discontinuous vector of sliding modes for the subsystem i, defined by

$$\varphi_i(t) = E_{fi} sign(P_i \tilde{e}(t)), \tag{4.29}$$

where the sign function of $P_i \tilde{e}(t)$ is calculated element by element, $E_{fi} > 0$ a positive constant, $P_i > 0$ satisfies the Lyapunov equation, and the estimated state error $\tilde{e}$ is defined by

$$\tilde{e} = x(t) - \hat{x}(t). \tag{4.30}$$

4.4.3 Sliding-Mode Takagi-Sugeno fuzzy observer

From the Takagi-Sugeno observer presented in (4.24), according to Castillo et al. (2005), the corresponding sliding-mode Takagi-Sugeno fuzzy observer is defined by

$$\begin{aligned} \dot{\hat{x}}(t) &= \sum_{i=1}^{r} h_i(z(t))(A_i\hat{x}(t) + B_iu(t) + K_i(e) + \varphi_{TSi}(t)) \\ \hat{y}(t) &= \sum_{i=1}^{r} h_i(z(t))(C\hat{x}(t)). \end{aligned} \tag{4.31}$$

with the sliding vector $\varphi_{TSi}(t)$ is defined as

$$\varphi_{TSi}^{T}(t) = sign(\dot{\tilde{e}}^{T} P_i). \tag{4.32}$$

is considered as the product between the estimation error derivative $\dot{\tilde{e}}$ and a positive definite matrix P_i, where the dynamic estimation error corresponds to the difference between the dynamic measured states of the system and the dynamic states estimated by the sliding-mode fuzzy observer, as expressed in

$$\dot{\tilde{e}} = \dot{x}(t) - \dot{\hat{x}}(t). \tag{4.33}$$

Since we are interested in the error approaching zero as t approaches infinity. According to the analysis and design characteristics between the fuzzy observer and the sliding-mode fuzzy observer, the stability and the matrix P are determined as in (4.25) and the gains K_i as in (4.26).

4.5 Design of the sliding-mode Takagi-Sugeno fuzzy observer for the boiler heating actuator

As mentioned, the buck-boost converter is the boiler heating actuator. According to the Takagi-Sugeno fuzzy model for the buck-boost converter defined in (4.22), the corresponding fuzzy observer is defined by

$$\begin{aligned} \dot{\hat{x}} &= Ax(t) + \left(\sum_{i=1}^{4} h_i(z_1, z_2)B_i + \varphi_{TSi}(t) \right) d \\ y(t) &= \sum_{i=1}^{4} h_i(z_1, z_2)Cx(t). \end{aligned} \tag{4.34}$$

The output matrix C is defined by

$$C_{=} \begin{pmatrix} 1 & 0 \\ 0 & 1 \end{pmatrix}, \tag{4.35}$$

where the system outputs are v_C and i_L.

The block diagram of the buck-boost converter observer is shown in Fig. 4.13, where the fuzzy variables (z_1, z_2) are the states of the system ($x_1 = v_C$, $x_2 = i_L$), and the gains of the fuzzy observer are defined as K_f and K_ϕ.

According to the characteristics of the fuzzy model of the converter presented in (4.22), where the state matrices A_1, A_2, A_3 and A_4 are identical, the LMI that guarantees the stability of the sliding-mode

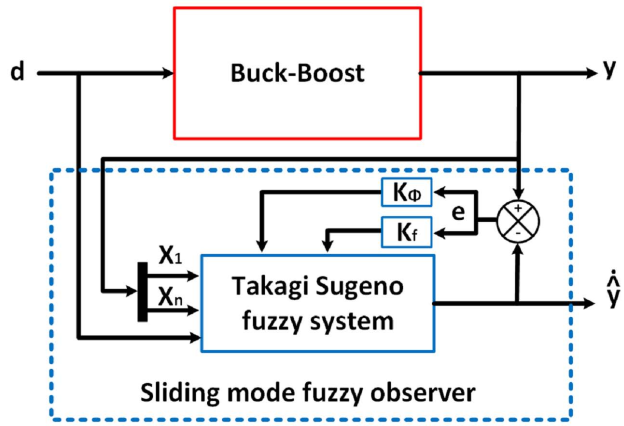

Fig. 4.13: Sliding-mode Takagi-Sugeno fuzzy observer for the buck-boost converter

fuzzy observer for the buck-boost converter is defined by

$$\begin{gathered} P_{\phi_a}\phi > 0 \\ A'P_{\phi_a} - C'N'_{\phi_a} + P_{\phi_a}A - N_{\phi_a}C < 0. \end{gathered} \tag{4.36}$$

Given the solution for P_{ϕ_a}, the gain K_ϕ for the observer is determined by

$$K_\phi = P_{\phi_a}^{-1} N_{\phi_a}. \tag{4.37}$$

4.5.1 Validation of the sliding-mode Takagi-Sugeno fuzzy observer for the heating actuator

The buck-boost converter (boiler heating actuator) observer is validated in simulation considering the converter characteristics presented in Table 4.1. Figure 4.14 shows the observer convergence to the capacitor voltage v_C under disturbances in the nominal input voltage ($V_{in} = 180$ V). In the observer simulation at 0.1 s the input voltage V_{in} decreases 8.88% ($V_{in} = 160$ V) of its nominal value. At 0.2 s it increases 111.11% ($V_{in} = 200$ V) of its nominal value. In both cases it is shown that the observer ($\hat{v_C}$) converges to the capacitor voltage v_C measured in the real system. The observer presents a maximum estimation error of 1.3 V and a minimum of 100 μ V.

Figure 4.15 shows the observer convergence to the inductor current i_L under disturbances in the nominal input voltage ($V_{in} = 180V$). In 0.1 s the voltage V_{in} decreases 88.88% to $V_{in} = 160$ V, and in 0.2 s it increases 111.11% $V_{in} = 200$ V. In both cases, it is shown that the observer $\hat{i}_L$ converges to the inductor current i_L of the nonlinear model. The observer presents a maximum estimation error of 394 mA and a minimum error of 80 μA.

Figure 4.16 shows the observer's convergence to the capacitor voltage under variations in the nominal load ($R_L = 70.3\ \Omega$). At 0.1 s the load decreases 78.23% ($R_L = 55\ \Omega$), and at 0.2 s it increases 113.79%

Table 4.1: Parameter of the buck-boost converter

Parameter	Magnitude
Input voltage (V_{cc})	$180V$
Output voltage (V_{out})	$-229V$
Inductor (L)	$5\mu H$
Capacitor (C)	$78\mu F$
Load (R_L)	70.3Ω
Frequency (f)	20 kHz
Duty cycle (d)	0.56

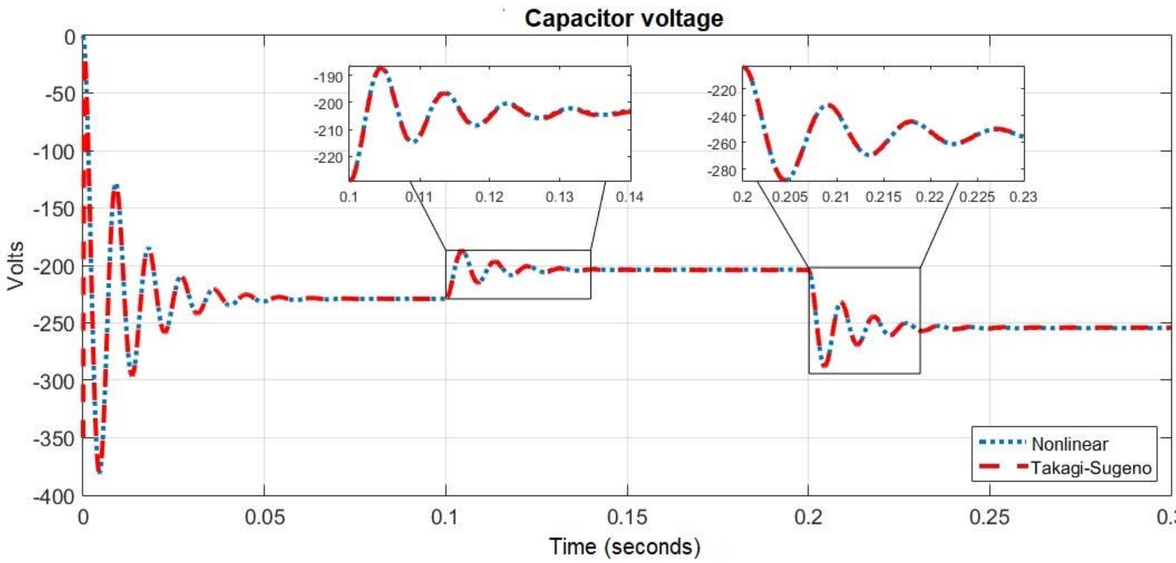

Fig. 4.14: Observer response in the capacitor voltage v_C under disturbances in the input voltage V_{in}

($R_L = 80\ \Omega$). In both cases the observer ($\dot{\hat{i}}_L$) converges to the capacitor voltage v_C of the nonlinear model. The observer has a maximum error of 1 V and a minimum error of 75 μV.

Figure 4.17 shows the observer's convergence to the inductor current i_L under variations in the nominal magnitude of the load ($R_L = 70.3\ \Omega$). At 0.1 s the load decreases 78.23% ($R_L = 55\ \Omega$), and at 0.2 s it increases 113.79% ($R_L = 80\ \Omega$). In both cases, the observer converges to the inductor current. The observer presents a maximum error of 13 mA and a minimum error of 100 μA.

As can be observed, the estimated states by the fuzzy observer for the boiler actuator converges adequately to the real states of the system under perturbations, allowing designing and implementing a fault detection and diagnosis systems based on analytical redundancy.

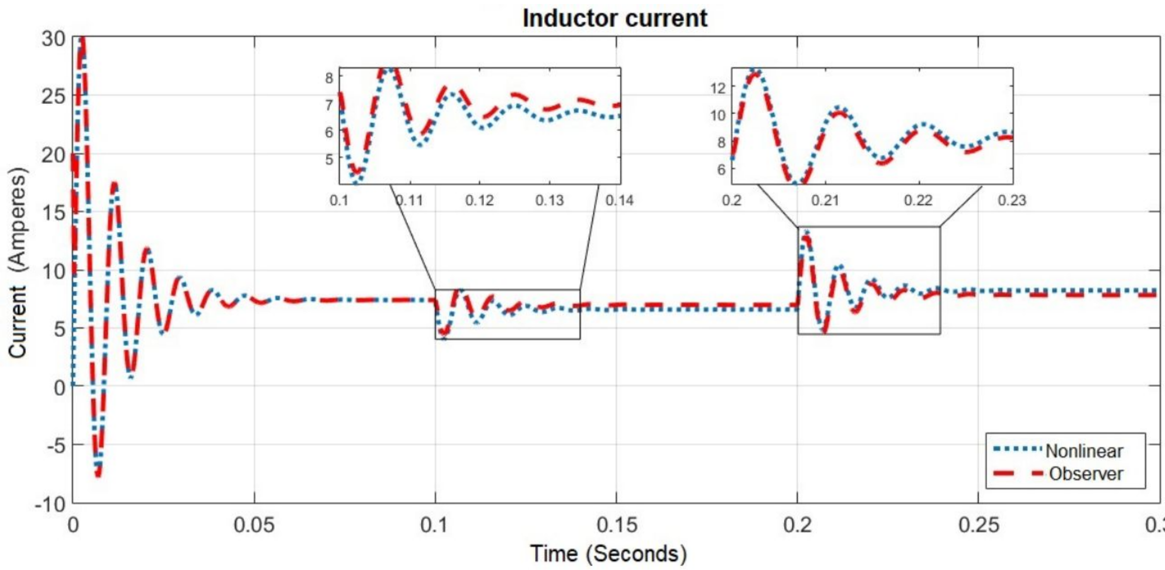

Fig. 4.15: Observer response for the inductor current i_L under disturbances in the input voltage V_{in}

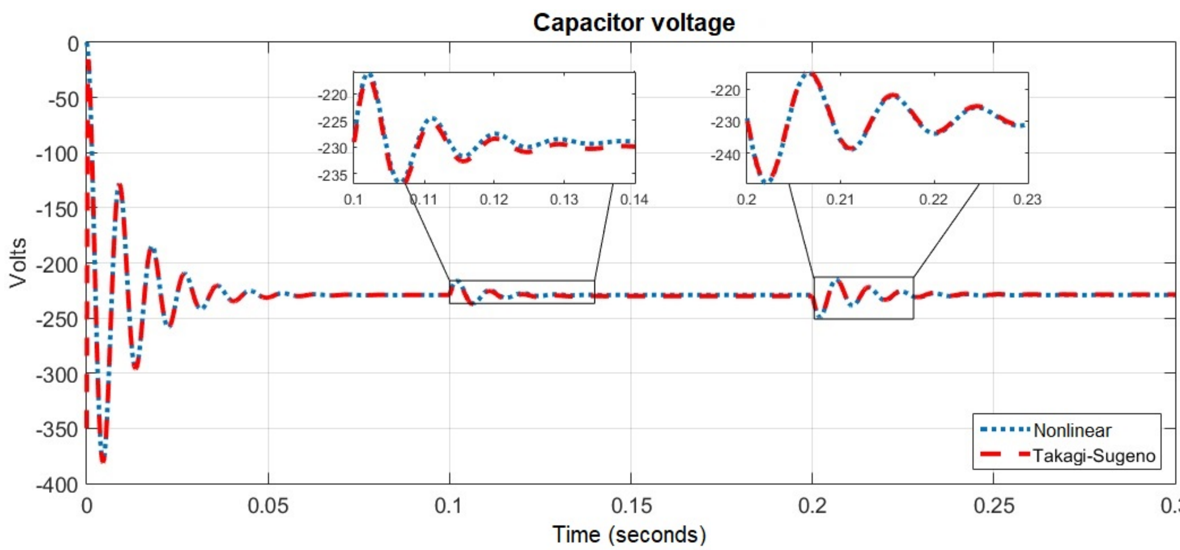

Fig. 4.16: Observer response for the capacitor voltage v_C under load variations R

4.5.2 Fault detection for the boiler heating actuator

The block diagram of the FDI system for the boiler heating actuator for the distillation column is shown in Fig. 4.18.

The FDI system for the heating actuator is based on a bank of two fuzzy observers. The inputs are the inductor current i_L for Observer 1 and the capacitor voltage v_C for Observer 2. The difference between the estimates of both observers allows detecting and diagnosing the type of fault in the converter. The difference between the estimates of both observers allows detecting and diagnosing the faults in the converter. The four generated residuals are

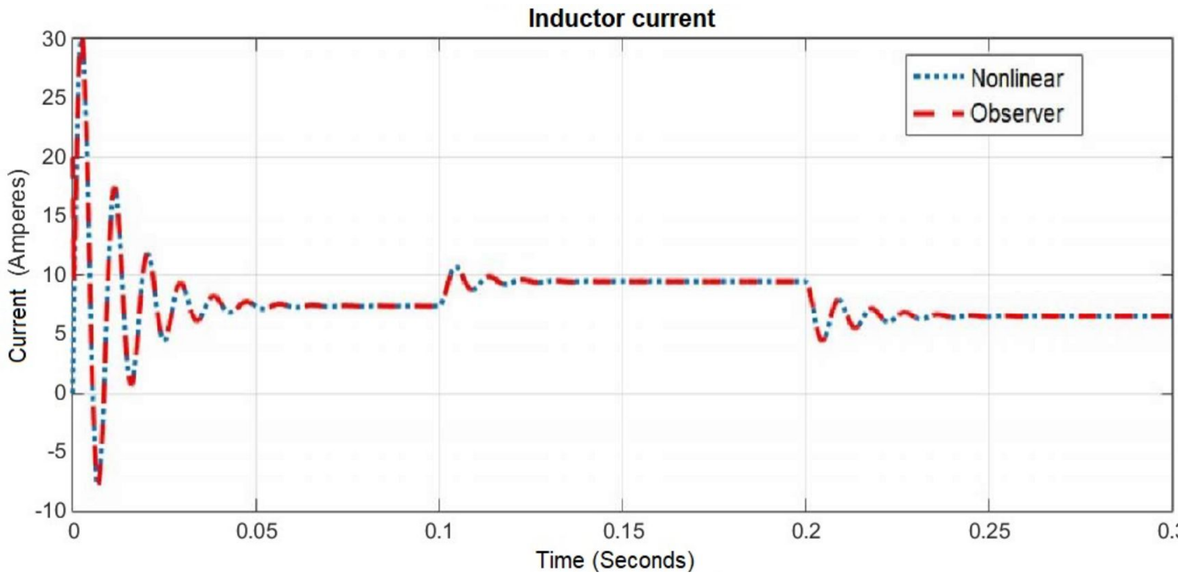

Fig. 4.17: Observer response in the inductor current i_L under load variations R

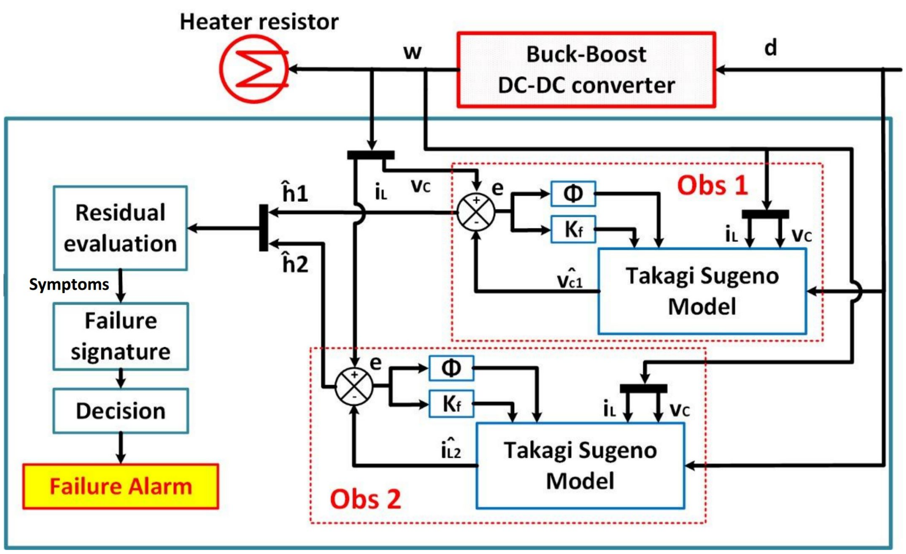

Fig. 4.18: FDI system for the boiler heating actuator

$$\begin{array}{ll} r_{i_L 1} = i_L - \hat{i}_{LO1}, & r_{v_C 1} = v_C - \hat{v}_{CO1} \\ r_{i_L 2} = i_L - \hat{i}_{LO2}, & r_{v_C 2} = v_C - \hat{v}_{CO2}, \end{array} \tag{4.38}$$

where $\hat{i}_{L0i}$ and $\hat{v}_{CL0i}$ for $i = 1,2$ are the outputs estimated by the observers. The residuals evaluation provides the symptoms for the diagnosis of the faults in the converter according to the fault signature presented in Table 4.2.

The FDI system detects faults in the nominal load R_L. Furthermore, it is sensitive to variations in the nominal supply voltage V_{cc}, detecting the conditions and faults below.

Table 4.2: Fault signature

Fault	F1	F2	F3	F4	F5	F6	F7	F8
r_{i_L1}	-1	0	1	-1	1	-1	1	-1
r_{i_L2}	0	0	1	-1	1	- 1	1	0
r_{v_C1}	1	-1	1	-1	1	-1	1	-1
r_{v_C2}	1	-1	0	0	1	-1	-1	1

- F1: Decrease in the nominal supply voltage of the converter V_{cc}
- F2: Increase in the nominal supply voltage of the converter V_{cc}
- F3: Decrease in the magnitude of the nominal load R_L
- F4: Increase in the magnitude of the nominal load R_L
- F5: Decrease in the nominal power supply voltage of the converter V_{cc} and decrease in the magnitude of the nominal load R_L
- F6: Increase in the nominal power supply voltage of the converter V_{cc} and increase in the magnitude of the nominal load R_L
- F7: Increase in the nominal power supply voltage of the converter V_{cc} and decrease in the magnitude of the nominal load R_L
- F8: Decrease in the nominal power supply voltage of the converter V_{cc} and increase in the magnitude of the nominal load R_L

4.6 Experimental validation of the FDI system

The experimental validation of the FDI system is performed for a buck-boost converter that regulates the voltage to a heating resistance of 350 W for the EDF-1000 distillation column boiler. The observer design parameters for the FDI system are determined for the case study presented in Table 4.1.

The FDI system is designed assuming that variations in the converter input voltage are caused mainly by the input voltage (line voltage) resulting in thermal shocks if the power supplied to the boiler increases or the slowness of the process dynamics if the power supplied in the heating resistance is low. Load variations are usually caused by degradation or manufacturing of the heating resistance.

The structure of the observer system for the buck-boost converter is expressed by

$$\begin{aligned} \dot{x}(t) &= Ax(t) + \left(\sum_{i=1}^{4} h_i(z_1,z_2)B_i\right) d(t) \\ y(t) &= \sum_{i=1}^{4} h_i(z_1,z_2)C_i x(t). \end{aligned} \tag{4.39}$$

According to the characteristics of the fuzzy system, where $A_1, A_2, A_3, A_4 = A$, the LMIs to determine the stability of the system are given by

$$\begin{aligned} P &> 0 \\ A^T P - C^T N^T + PA - NC &< 0. \end{aligned} \tag{4.40}$$

Thus, given the solution for P, the observer gain K is determined by

$$K = P^{-1}N. \tag{4.41}$$

The FDI experimental validation for the process presented in Table 4.1 considers faults in the nominal load value, variations in the converter input voltage and the combination of both simultaneous faults.

4.6.1 Test 1: Load decrease

In order to validate the FDI behavior under heating resistance variations, a decrease of 50% of its nominal value (38 Ω) occurs at $0.1s$.

Figure 4.19 presents the observers' dynamics when the load decrease fault occurs. The observer with the i_L reference, Observer 1, presents a greater difference concerning the capacitor voltage value when a load decrease occurs, causing a residue of greater magnitude with respect to the observer with the v_C reference, Observer 2.

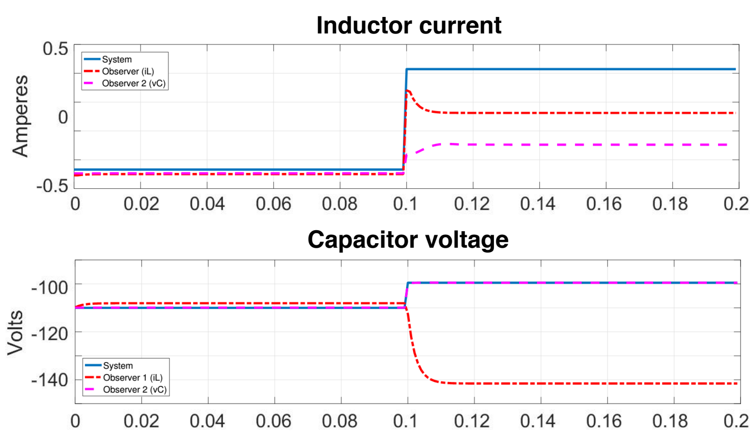

Fig. 4.19: Observers' estimation concerning a nominal load decrease

Figure 4.20 shows the residuals generated without fault from 0 to 0.1 s and under a fault's presence after 0.1 s. It can be observed that the residuals generated by Observer 1, with the i_L reference, exceed the decision thresholds, fixed experimentally according to the process dynamics, after the load decrease.

Figure 4.21 shows the symptoms generated when evaluating the residuals with the defined thresholds. According to the Table 4.2, the FDI system adequately identifies the F3 fault (nominal load decrease).

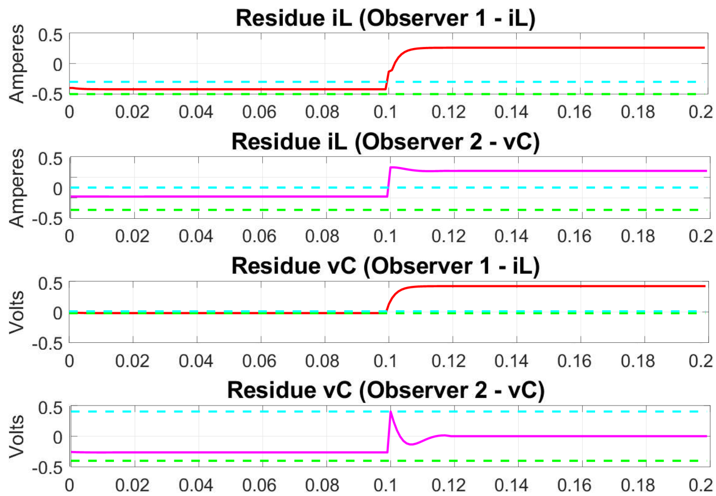

Fig. 4.20: Residuals compared to the fixed decision thresholds under a nominal load decrease

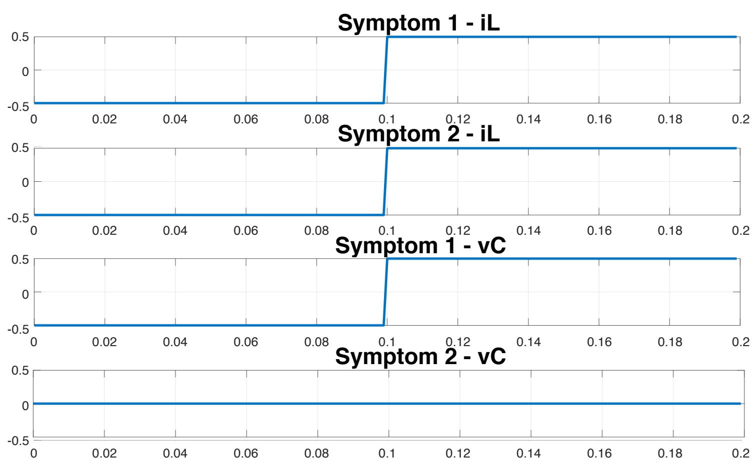

Fig. 4.21: Symptoms obtained under a nominal load decrease

4.6.2 Test 2: Input voltage decrease

In the second validation test, a disturbance in the input voltage is considered. A 16.66% decrease from its nominal value is generated at 0.1 s. Figure 4.22 shows that Observer 1 has a greater difference considering the inductor current and the capacitor voltage that Observer 2.

Figure 4.23 shows the residuals generated without fault from 0 to 0.1 s and under an input voltage decrease after 0.1 s. It can be observed that only the residuals generated by Observer 2 for the inductor current are minor than the decision thresholds fixed experimentally according to the process dynamics.

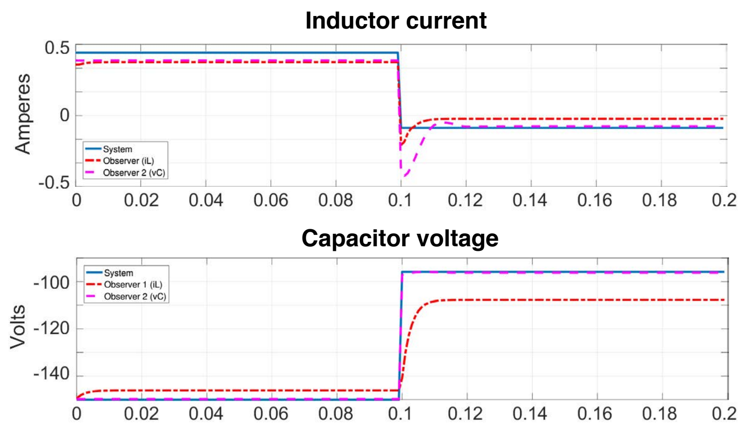

Fig. 4.22: Estimation using observer 1 and 2 considering an input voltage decrease

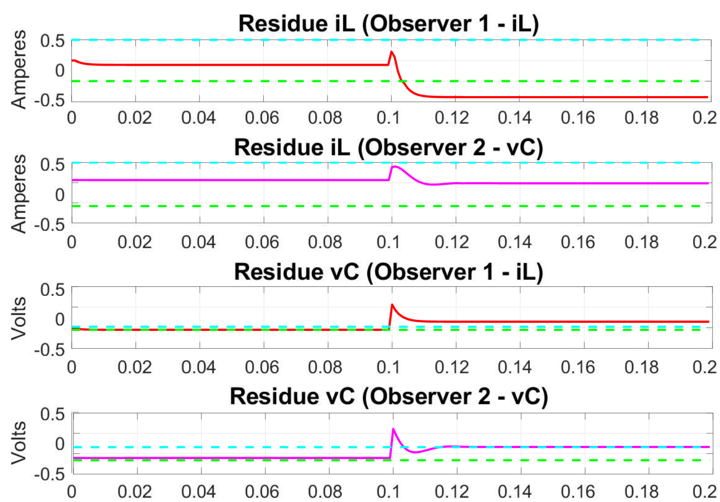

Fig. 4.23: Residuals compared to the fixed decision thresholds under an input voltage decrease

Figure 4.24 shows the symptoms generated when evaluating the residuals with the defined thresholds, and it can be observed that at 0.1 s the magnitude of the symptoms changes according to the difference between the observers estimation with respect to the real value. Symptom 2 for the v_C obtained by Observer 2 has a transient response that switches between 0 and 1 because the response of Observer 2 for the inductor current i_L presents an overdamped transient response. By evaluating the symptoms and according to Table 4.2 it can be determined that a fault exists, which corresponds to a decrease in the input voltage.

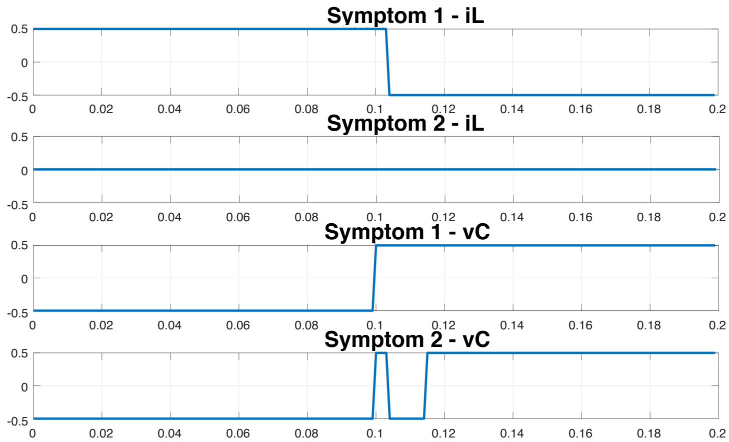

Fig. 4.24: Symptoms obtained under an input voltage decrease

4.6.3 Test 3: Simultaneous faults

A third experiment is performed where a 50% increase in the nominal value of the load in addition to a 16.6% increase in the actuator input voltage. Figure 4.25 shows the dynamics of the observers.

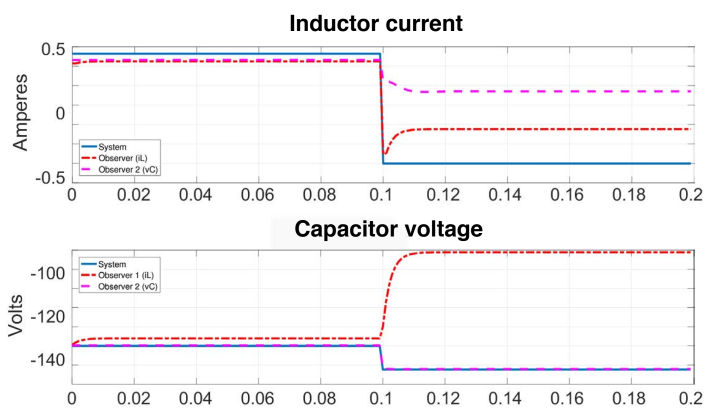

Fig. 4.25: Observers' estimation concerning under an input voltage and load decrease

At $0.1s$ the combined fault is presented. Both observers lose convergence with the inductor current, i_L. Observer 2 maintains convergence with the capacitor voltage despite the multiple faults. Figure 4.26 shows the residuals obtained for each observer estimation under multiple faults in the system.

The generated residuals show similar behavior with difference values below the selected thresholds. Accordingly, the symptoms that appear in Fig. 4.27 are all negative. By comparing these signatures with

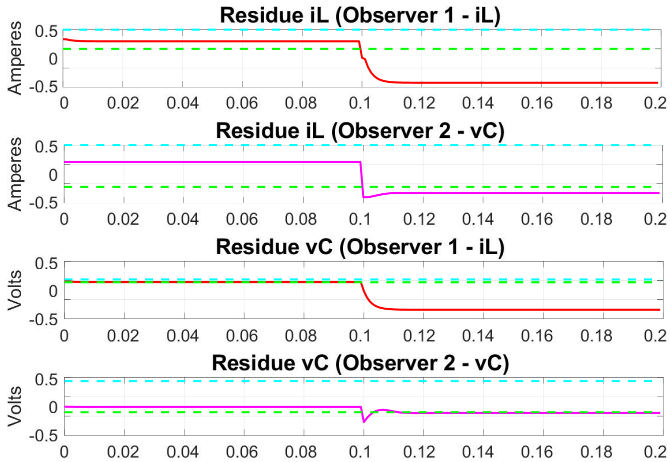

Fig. 4.26: Residuals obtained under an input voltage and load decrease

the fault shown in Table 4.2, it can be concluded that a multiple fault corresponding to the combination of load and input voltage increases exists.

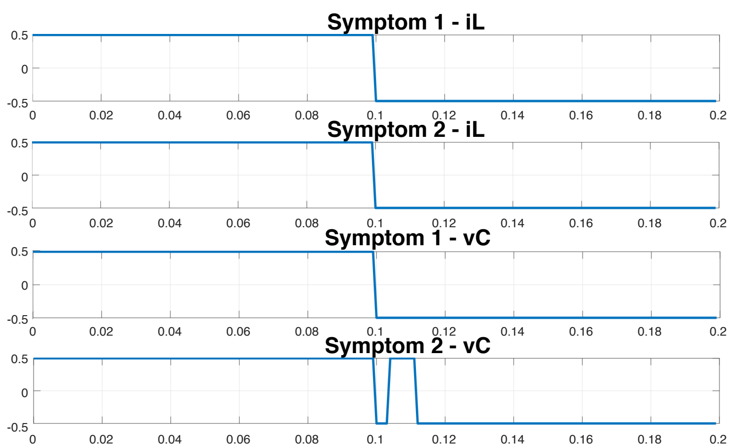

Fig. 4.27: Symptoms obtained under simultaneous input voltage and load decrease

4.7 Conclusions

In this chapter, an FDI system for a buck-boost converter acting as the boiler heating actuator for the EDF-1000 distillation pilot plant was implemented. The buck-boost converter function is to regulate the electrical power W of a heating resistance through its duty cycle d. For the FDI system, two sliding-mode

Takagi-Sugeno fuzzy observers were designed, both observers estimate the converter output voltage v_C and the inductor current, i_L.

This FDI system allows obtaining four residuals, $r_{i_L 1}$, $r_{i_L 2}$, $r_{v_C 1}$ and $r_{v_C 2}$, which determine the symptoms to indicate the presence or absence of faults.

According to the results obtained in simulation and in experimentation, the observers with sliding modes have acceptable results with small convergence times, around 800 µs.

It is feasible to experimentally design an FDI scheme for an EDF-100 distillation pilot plant modeled by a Takagi-Sugeno type structure and techniques based on the model, such as the use of observers with sliding modes.

This page intentionally left blank

References

Kumar, A., Bhattacharya, A. and Flores-Cerrillo J.F. (2020). Data-driven process monitoring and fault analysis of reformer units in hydrogen plants: Industrial application and perspectives. In *Computers & Chemical Engineering*. Volume 136, 106756. Elsevier

Affam, A., Buswig, Y. M., Othman, A. K. B. H., Julai, N. B., & Qays, O. (2021). A review of multiple input DC-DC converter topologies linked with hybrid electric vehicles and renewable energy systems. In *Renewable and Sustainable Energy Reviews*, Volume 135, 110186.

Bahreini, M., Zarei, J., Razavi-Far, R., and Saif, M. (2021). Robust and reliable output feedback control for uncertain networked control systems against actuator faults. In *IEEE Transactions on Systems, Man, and Cybernetics: Systems*, 52(4), 2555-2564.

Téllez-Anguiano, A. C., Heras-Cervantes, M., Anzurez-Marín, J., Chávez-Campos, G. M., and Gnecchi, J. A. G. (2017). Mathematical modelling of batch distillation columns: A comparative analysis of non-linear and fuzzy models. IntechOpen.

Demidova, G., Rassõlkin, A., Vaimann, T., Kallaste, A., Zakis, J. and Suzdalenko, A. (2021). An Overview of Fuzzy Logic Approaches for Fault Diagnosis in Energy Conversion Devices. In *2021 28th International Workshop on Electric Drives: Improving Reliability of Electric Drives (IWED)*. pages 1–7, IEEE.

Heras-Cervantes, M., Anzurez-Marin, J., del Carmen Téllez-Anguiano, A., del Carmen García-Ramírez, M., and Correa-Gómez, J. (2016). Modelling a heating-power actuator for a distillation column boiler. pages 1–6. IEEE.

Li, Y., Sun, Y., Gao, Y., Sun, J., Lyu, H. F., Yu, T., and Wang, Y. (2022). Analysis of overload induced arc formation and beads characteristics in a residential electrical cable. *Fire Safety Journal*, 131, 103626.

Ibrahim, D., Jobson, M., Li, J., and Guillén-Gosálbez, G. (2018). Optimization-based design of crude oil distillation units using surrogate column models and a support vector machine. *Chemical Engineering Research and Design*, 134:212–225.

Iqbal, R., Maniak, T., Doctor, F. and Karyotis C. (2019). Fault Detection and Isolation in Industrial Processes Using Deep Learning Approaches. *IEEE Transactions on Industrial Informatics*, volume 15, 5:3077-3084.

Kordestani, M., Saif, M., Orchard, M. E., Razavi-Far, R. and Khorasani, K. (2019). Failure prognosis and applications—A survey of recent literature. In *IEEE transactions on reliability*, volume 70, number 2, pages 728–748. IEEE.

Khan, A. S., Khan, A. Q., Iqbal, N., Sarwar, M., Mahmood, A., and Shoaib, M. A. (2020). Distributed fault detection and isolation in second order networked systems in a cyber–physical environment. *ISA transactions*, 103:131–142.

Lopez, F.-R., Ponsart, J.-C., Theilliol, D., Astorga-Zaragoza, C., and Flores-Montiel, M. (2015). Robust state and fault estimation observer for discrete-time d-lpv systems with unmeasurable gain scheduling functions. application to a binary distillation column. *IFAC-PapersOnLine*, 48(21):1012–1017.

Ming, L. and Zhao, J. (2017). Review on chemical process fault detection and diagnosis. In *2017 6th International Symposium on Advanced Control of Industrial Processes (AdCONIP)*, pages 457–462. IEEE.

Orozco, G., Cortés, B., Heras, M., Téllez, A., and Anzurez, J. (2016). Analysis and comparison of distillation column models considering constant and variable relative volatility. pages 1–6. IEEE.

Paraschiv, N. and Olteanu, M. (2015). Feedforward process control of a distillation column based on evolutionary techniques. In *System Theory, Control and Computing (ICSTCC), 2015 19th International Conference on*, pages 730–735. IEEE.

Rashid, M. H. (2017). *Power electronics handbook*. Butterworth-Heinemann.

Rojas, C. A., Kouro, S., Perez, M. A., and Echeverria, J. (2018). Dc-dc mmc for hvdc grid interface of utility-scale photovoltaic conversion systems. *IEEE Transactions on Industrial Electronics*, 65(1):352–362.

Alhaboubi, N. A. (2022). Constant distillate composition of batch distillation column with variable reflux mode based on still pot concentration. In *Science and Technology for Energy Transition*, 77, 2.

Skogestad, S. (1997). Dynamics and control of distillation columns: A tutorial introduction. *Chemical Engineering Research and Design*, 75(6):539–562.

Tanaka, K., Ikeda, T., and Wang, H. O. (1998). Fuzzy regulators and fuzzy observers: relaxed stability conditions and lmi-based designs. *IEEE Transactions on fuzzy systems*, 6(2):250–265.

Nguyen, A. T., Taniguchi, T., Eciolaza, L., Campos, V., Palhares, R., and Sugeno, M. (2019). Fuzzy control systems: Past, present and future. *IEEE Computational Intelligence Magazine*, 14(1), 56-68.

Tarakanath, K., Patwardhan, S., and Agarwal, V. (2014). Internal model control of dc-dc boost converter exhibiting non-minimum phase behavior. pages 1–7. IEEE.

Téllez, A. (2010). *Supervisión Electrónica de Columnas de Destilación Basada en Modelos*. PhD thesis, Centro Nacional de Investigación y Desarrollo Tecnológico, Departamento de Ingeniería Mecatrónica.

Verde, C., Gentil, S., and Morales-Menéndez, R. (2013). *Monitoreo y diagnóstico automático de fallas en sistemas dinámicos*. Trillas.

Zhong, W., Lu, J., and Miao, Y. (2017). Fault detection observer design for fractional-order systems. In *2017 29th Chinese Control And Decision Conference (CCDC)*, pages 2796–2801. IEEE.

Castillo-Toledo, B., and Anzurez-Marin, J. (2005, June). Model-based fault diagnosis using sliding mode observers to Takagi-Sugeno fuzzy model. In *Proceedings of the 2005 IEEE International Symposium on, Mediterrean Conference on Control and Automation Intelligent Control*, pp. 652-657. IEEE.

Chaouech, L., Soltani, M., and Chaari, A. (2019). Fuzzy sliding mode controller design using scalar sign function for a class of TS fuzzy models. In *2019 6th International Conference on Control, Decision and Information Technologies (CoDIT)*, pp. 1823-1828. IEEE.